

Broadband phase and intensity compensation with a deformable mirror for an interferometric nuller

Robert D. Peters,* Oliver. P. Lay, and Muthu Jeganathan

Jet Propulsion Laboratory, California Institute of Technology, 4800 Oak Grove Drive,
Pasadena, California 91109 USA

*Corresponding author: Robert.D.Peters@jpl.nasa.gov

Received 26 March 2008; revised 9 June 2008; accepted 13 June 2008;
posted 16 June 2008 (Doc. ID 94240); published 17 July 2008

Nulling interferometry has been proposed for the direct detection of Earth-like planets. Deep stable nulls require careful control of the relative intensity and phase of the beams that are being combined. We present a novel compensator, the Adaptive Nuller, that corrects the intensity and phase as a function of wavelength from 8 to 12 μm using a deformable mirror. This compensator has been used to produce rejection ratios of 82000:1 over a bandwidth of 3.2 μm centered around 10 μm . © 2008 Optical Society of America

OCIS codes: 120.3180, 120.4570.

1. Introduction

Direct detection of Earth-like planets around nearby stars requires a combination of starlight suppression and high angular resolution (<0.1 arcsec). An approach to starlight suppression at mid-IR wavelengths, termed nulling interferometry [1], has been proposed for both the European Darwin mission [2] and NASA's Terrestrial Planet Finder Interferometer (TPF-I) [3,4].

A schematic nulling interferometer is shown in Fig. 1. Two telescopes observe a star that has a planet in orbit around it. The goal is to combine the light from the two telescopes in antiphase such that we obtain a null in the instrument response at the position of the star. The wavefront from the star is incident on the collecting apertures of the instrument and delivered by the respective beam trains to a central beam combiner that couples the light into a single-mode spatial filter (SMSF) as shown at the bottom of Fig. 1. The SMSF removes these spatial wavefront errors, which in a real interferometer would limit the rejection by the wavefront errors introduced due to imperfect optics in the interferometer. All designs of TPF-I

and Darwin under consideration have included a SMSF through which the combined light is passed before being detected.

The electric fields from each telescope in the SMSF must have equal amplitudes and phases that differ by π radians to create the response on the sky as shown at the top of the figure. This requirement must be met simultaneously for both horizontal and vertical polarization states and for all wavelengths across the science bandwidth, which for TPF-I is approximately 7–17 μm . This ideal null requires that the beam trains are perfectly symmetric and the π phase shift is achromatic [5]. An imbalance in intensity δI or phase $\delta\phi$ between the two arms results in a limiting null depth of $N \approx 1/4(\delta I^2 + \delta\phi^2)$. Therefore, the starlight is rejected by a factor of 10^5 if the amplitudes are balanced at the 0.1% level (intensities equal to within 0.2%) and phases are matched to within 0.3 mrad (5 nm at a wavelength of 10 μm).

With just a single mode for each polarization state, the problem of nulling the on-axis light is thus simplified. The electric field within the SMSF is the vector sum of the electric field contributions from each collecting aperture. The starlight would be completely nulled if the electric fields in the SMSF sum to zero. The degree to which this ideal can be met will

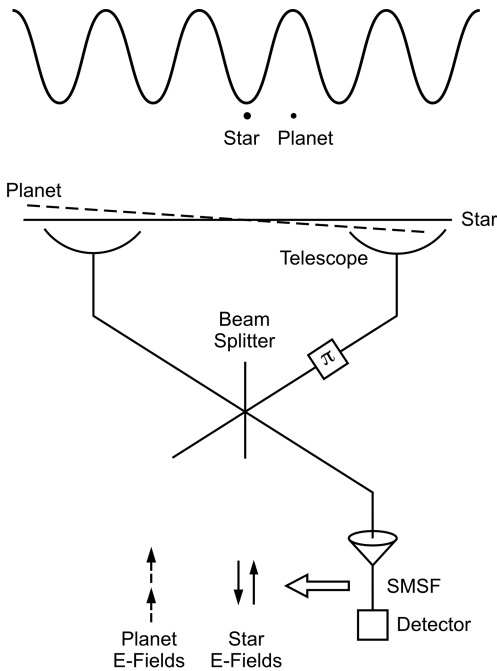


Fig. 1. Schematic starlight nulling pair used in the Terrestrial Planet Finder. The interference between the two telescopes creates a response pattern on the sky of constructive and destructive fringes. The star is located in the central destructive fringe, and the planet appears in the constructive fringe.

determine the performance of the nulling interferometer. A number of effects can perturb the amplitude coupling into the SMSF. These include the reflectivity of the mirrors and transmissive optics, beam shear, and wavefront aberration (tilt, focus, astigmatism, coma, etc.) The electric field phase is a function of the optical path length but also changes due to birefringence and dispersion introduced by the ~ 30 optical elements present in each beam train of TPF-I or Darwin.

A brute-force approach to designing the instrument would be to make the beam trains as identical as possible by applying extremely tight requirements to the alignment and specification of the optical elements. Error budgeting shows that the tolerances involved are prohibitive. Our solution is a technique we call Adaptive Nulling in which a compensator is included in each beam train to correct for imbalances in the amplitude and phase independently at each wavelength and in each polarization.

The technology demonstration described in this paper, showing the quasi-static control of phase dispersion and intensity dispersion, was chosen to be consistent with a 100,000:1 null depth, which is the flight requirement for TPF-I [6]. Phase control of 5 nm root mean square (RMS) and intensity control of 0.2% RMS would yield a null of 100,000:1 in the absence of dynamic sources of null degradation. This level of performance was deemed to be sufficiently challenging to serve as a convincing demonstration of the viability of adaptive nulling.

Here we describe an adaptive nulling compensator based on a deformable mirror. The concept is outlined in Section 2. In Section 3 we describe our method of testing the compensator to show that it will meet our requirements. The results of the laboratory testing are then presented in Section 4.

2. Adaptive Nulling Concept

The Adaptive Nuller uses a deformable mirror (DM) with a continuous face sheet to apply a high order independent adjustment of amplitude and phase prior to injecting the combined light into a single-mode filter. A schematic of the Adaptive Nuller is shown in Fig. 2, as it would be used to adjust the intensity and phase of one beam in a two-beam nuller. The incident beam is first split into its two linear polarization components, and then dispersed by wavelength. These beams are then focused onto the DM. Each actuator independently adjusts the phase and intensity of part of the dispersed spectrum. The dispersed spectrum of each polarization is then recombined to yield an output beam that has been carefully tuned for intensity and phase in each polarization as a function of wavelength.

The correction of the amplitude and phase for each polarization and at each wavelength is illustrated in Fig. 3. The piston of the DM actuator adjusts the phase of the output beam [Fig. 3(a)]; changing the local slope orthogonal to the dispersion direction of the DM at the focal point introduces a shear of the outgoing collimated beam, which is then converted into a reduction of amplitude in the SMSF [Fig. 3(b)]. The piston and local slope are adjusted independently for the different wavelengths and polarizations.

This compensator is part of a control system for balancing the amplitudes and phases of the incoming beams. Also needed is a sensor for detecting the imbalances and an algorithm to make the appropriate adjustment at the DM. In this system we share time on the science camera to measure the imbalances of phase and intensity which we estimate will require about 5% of the observation time. The advantages of this method are that there are no additional sensors needed, there are no uncommon path effects, and the science star is used as the calibration source which avoids changing the pointing of the array.

The Adaptive Nuller significantly relaxes the matching tolerances on optical components in the interferometer. Since it can be monitored and readily characterized, optical components need only be of sufficient quality that the two arms of the interferometer are matched in intensity and phase to within the capture range of the Adaptive Nuller. The ultimate null depth and stability are then determined by the performance of the Adaptive Nuller, the performance of the path length stabilization system, and polarization mixing. The amount of polarization mixing and the performance of the path length stabilization system are dependent on the optical design and are beyond the scope of this paper.

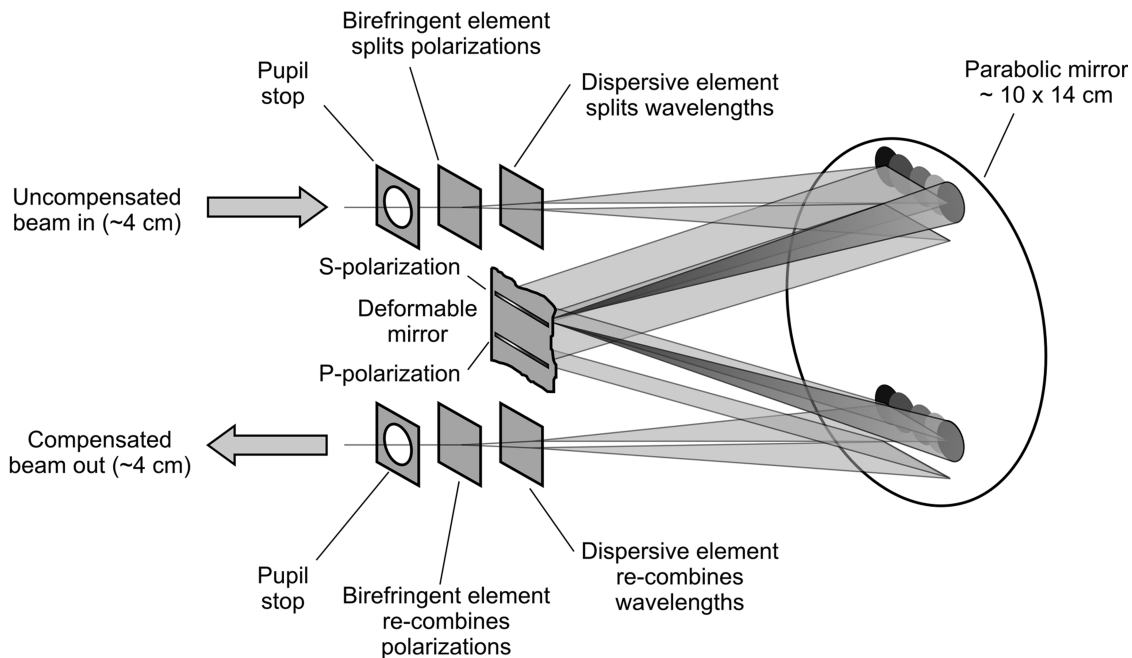


Fig. 2. Schematic of the Adaptive Nuller. Light in one arm of a nulling interferometer is balanced by splitting the polarizations and dispersing the wavelength, then adjusting the phases in each part of the spectrum with a deformable mirror prior to recombining the polarizations and wavelengths.

3. Laboratory Demonstration

The laboratory demonstration of the Adaptive Nuller used a Mach-Zehnder type interferometer as shown in Figs. 4 and 5. In one arm, we have the Adaptive Nuller as described above to adjust the phase dispersion and intensity imbalance. In the other arm, we have a copy of the Adaptive Nuller with a fixed reference mirror in place of the DM. A delay line consisting of a large retroreflector with two levels of actuation provides optical path length balance, and the combination of adjusting the Adaptive Nuller and delay line produce the achromatic π phase shift for the interferometer. The coarse actuation is accomplished by a computer controlled linear stage with 50 mm of travel and $0.1 \mu\text{m}$ resolution. The fine actuation is implemented with a piezoelectric actuator, which is coupled with a simple metrology system to remove air-path variations with a control bandwidth of 8 Hz. Finally, the outputs are recombined and sent through a SMSF before being detected by a spectro-

meter. The implementation of the source, Adaptive Nuller, and spectrometer are described below.

The input source to the interferometer consists of a ceramic heater collimated by an off-axis parabola. A small CO_2 laser is coaligned with the broadband thermal source to assist in alignment and calibration of the spectrometer. The source also contains a chopper wheel running near 1 kHz, which allows lock-in detection in the spectrometer. A small pinhole at the focus between two off-axis parabolas also provides some spatial filtering.

Wavelength separation and recombination in the Adaptive Nuller was accomplished with zinc selenide (ZnSe) wedges with an angle of 7° . The setup was modeled in Zemax, which predicted that the wavelengths would spread across 8 pixels of the DM. Polarization separation was not implemented in this demonstration. The source was unpolarized and both polarizations are controlled by the same set of actuators on the DM. However, a CdSe Wollaston prism was characterized independently of this demonstration [7] as having the desired properties and meeting specification requirements.

The Adaptive Nuller arm contains the DM as the correction actuator. We chose a 3 mm square 140 pixel Micro-Electro-Mechanical System DM from Boston Micromachines with a continuous thin gold-coated membrane that is deformed with electrostatic actuators driven by a custom digital high voltage controller system with 12 bit resolution. The light is focused onto the mirror such that it lies on one row of actuators. Actuation of this row and the row on either side is used to provide the tip and piston. The total stroke of any one actuator is approximately $2 \mu\text{m}$.

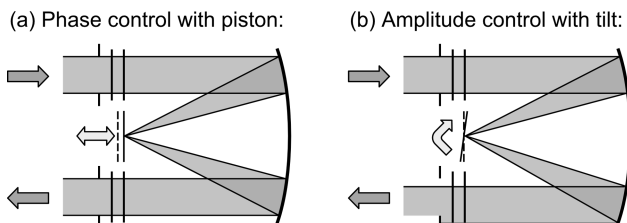


Fig. 3. (a) Side view of phase control with a single wavelength channel on the DM using piston. (b) Amplitude control of a single wavelength channel on the DM using tilt.

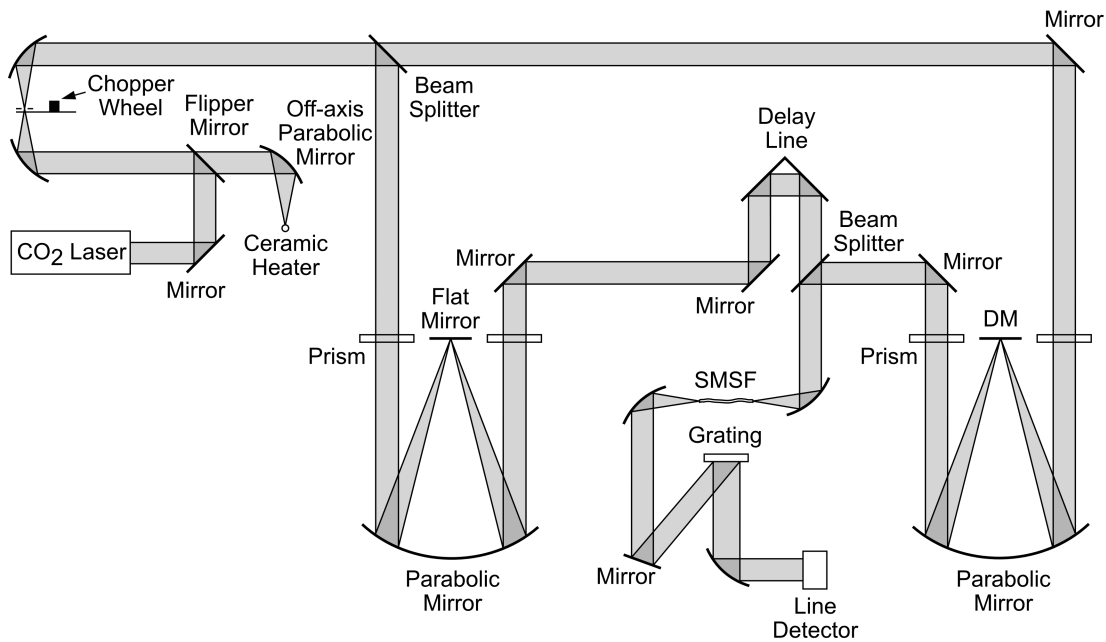


Fig. 4. Schematic layout for the mid-IR demonstration. The Adaptive Nuller is in one (right) arm, and a “reference” Adaptive Nuller in the other (left) arm. The reference has all the same optics as the Adaptive Nuller with the exception of a fixed mirror in place of the deformable mirror.

The output of the interferometer is coupled into a mid-IR SMSF obtained as part of a separate TPF-I technology development effort. This SMSF has been measured to reject modes other than the fundamental mode by at least 30 dB [8]. The signal is then detected by our spectrometer which takes the output of the SMSF and disperses the wavelengths with a reflective grating with 60 grooves/mm blazed for $10\ \mu\text{m}$. The 1st order reflection is focused by an off-axis parabola and detected by a sixteen element array HgCdTe detector. This detector array is scanned by an electronic multiplexer so that each pixel is measured sequentially by a lock-in amplifier. The output of the spectrometer is de-

tected intensity versus pixel. The known wavelengths from the CO₂ laser can be used to calibrate the spectrometer, and software converts the pixel position into wavelength.

Measurement of phase error requires that the delay line is offset to produce a channeled spectrum on the spectrometer. The spectrometer output is processed as outlined in the Appendix to produce the optical path difference (OPD) as a function of wavelength, from which the corrections to the DM actuators are calculated.

To measure the intensity error, a spectrum of each beam is taken by using a shutter to block the other beam off. The difference is divided by the sum of the two spectra to produce a measure of the intensity imbalance as a function of wavelength. Since the Adaptive Nuller can only decrease the light coupled into the SMSF, we must begin with an imbalance with more light in the Adaptive Nuller arm. We can use an adjustable iris to decrease the light in the reference arm.

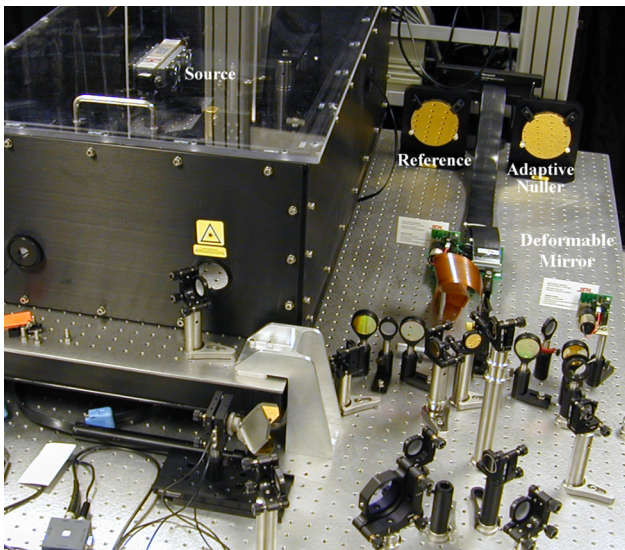


Fig. 5. (Color online) Picture of the laboratory setup showing the source and the two arms of the interferometer.

4. Laboratory Results

To demonstrate the repeatability of the results of the laboratory demonstration, three separate data sets were taken with several days of nonoperation in between. The dates and duration of each data set are shown in Table 1 and the data are presented in Figs. 6–11.

For each data set, we start with all actuators on the DM set to the same voltage. In the reference arm we placed an extra amount of ZnSe glass (to deliberately introduce a phase mismatch between the two arms) and adjusted the delay line to the central fringe. The intensity in the reference arm was decreased by

Table 1. Start Times and Duration for Each of the Three Data Sets Taken

Data Set	Date	Start	End	Duration
1	03/23/2007	6:05 pm	12:10 am (3/24/2007)	6 h 5 min
2	03/30/2007	2:36 pm	8:41 pm	6 h 5 min
3	04/06/2007	4:12 pm	10:13 pm	6 h 1 min

partially closing an adjustable aperture to deliberately introduce an intensity mismatch. We then measured the initial phase and intensity imbalance for the interferometer and applied the appropriate correction to the DM through the use of a simple proportional-integrator feedback loop. In our setup there is some amount of cross coupling between correcting the phase and intensity imbalance. As we iterate between phase and intensity correction, the system converges to within our requirement and the iterations are stopped. An improved model of the cross coupling and mirror influence function may reduce the number of iterations needed to converge. Figure 6 shows the RMS phase and intensity imbalance as a function of iteration.

Figures 7 and 8 show the intensity and phase imbalance before and after correction. The measurements before correction are made with the DM set with the same value on all actuators. The measurements after correction are made after iterating between phase and intensity correction until both values are

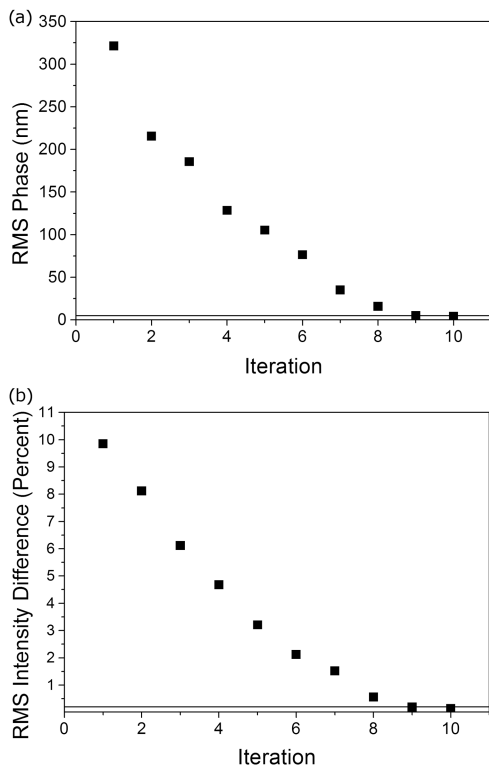


Fig. 6. RMS phase and intensity mismatch as a function of iteration. Because of cross coupling between the phase and the intensity adjustment as well as the influence function of the continuous face sheet, it takes several iterations to converge. This could potentially be improved by a better model of the mirror response.

below the TPF requirement (0.2% intensity and 5 nm RMS phase). These plots demonstrate that the Adaptive Nuller can correct large (~400 nm RMS) phase dispersions and wavelength dependent intensity imbalances (~9%) by about 2 orders of magnitude. This has a significant impact on the nulling performance of the interferometer. The uncorrected phase and intensity error would limit the inverse of the null depth to around 50:1, whereas the corrected phase and intensity would produce rejection ratios greater than 100,000:1 assuming no other error sources.

Figures 9 and 10 show the time evolution of the intensity and phase correction over a period of 6 h during which the DM actuators are held with a constant command value and no further corrections are made. These plots demonstrate the stability of the Adaptive Nuller.

To test the nulling performance, the corrections are applied to the phase and intensity imbalance. The null intensity is recorded for each pixel. The delay line is scanned slowly and the peak power obtained in each pixel is measured. The null depth shown in Fig. 11 is the ratio of the nulled intensity to peak power in each pixel. To assure we are not limited by the detector and

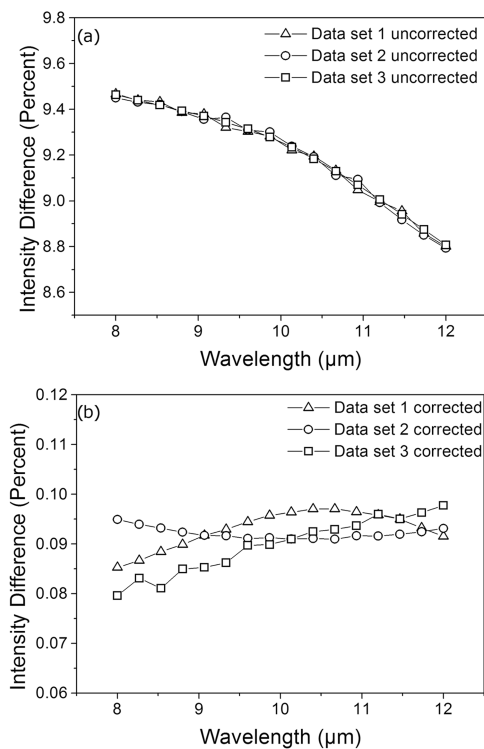


Fig. 7. Intensity dispersion for the three data sets taken (a) before the correction is applied and (b) after the correction is applied.

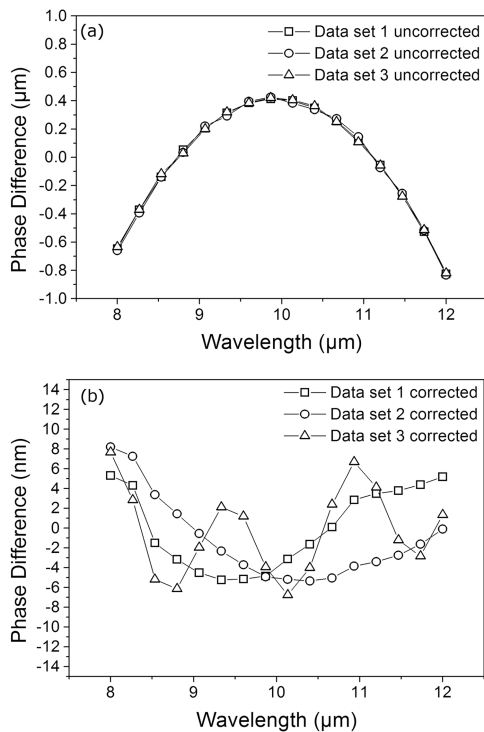


Fig. 8. Correction of the phase dispersion for each data set (a) before the correction was made and (b) after the correction was complete.

electronic noise, we take a dark frame which is shown as the detector noise plot in the figure. The RMS over wavelength of the null signal is 1.22×10^{-5} of the peak, which corresponds to a null of 82,000:1. For this data set, we had a measured intensity imbalance of 0.11%, and a phase dispersion of 2.8 nm, corresponding to a null depth of the order of 700,000:1 in the absence of any other error sources. The discrepancy can be accounted for by the dynamic fluctuations in the path difference—our path length metrology indicated uncorrected path length fluctuations of the order of 10 nm, corresponding to a theoretical null depth of 90,000:1.

5. Conclusion

The technique of adaptive nulling presented in this paper corrects for high order intensity and phase mismatches across the science band and requires no additional sensors beyond the science camera. This technique has the potential to significantly relax the requirements on the beam train optics within TPF-I, as well as the design of the nuller itself.

We have demonstrated that the technique can correct phase and intensity fluctuations by 2 orders of magnitude to below 5 nm phase and 0.1% in intensity difference. We have also demonstrated that these corrections are stable over 6 h in a laboratory environment. Nulls exceeding 80000:1 have been made with this technique in the mid-IR with a bandwidth of 3.2 μm centered on 10 μm.

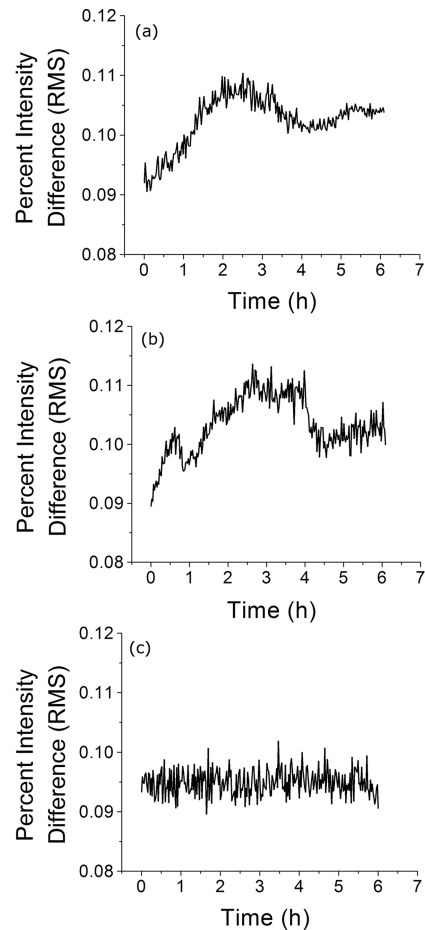


Fig. 9. RMS intensity stability as a function of time for data sets (a) 1, (b) 2, and (c) 3.

The nulling measurements appear to be limited by the path length fluctuations in the test bed. Reducing these fluctuations should allow even deeper nulls to be obtained. It is also possible that even better phase and intensity imbalance may be achieved by allowing the system to iterate beyond the specific requirement of the Terrestrial Planet Finder Interferometer.

Appendix A: Calculating Phase Error

Measuring phase error as a function of wavelength is accomplished using a variant of the Hilbert transform [9]. In this approach, the interferogram is measured on the spectrometer with an optical path length offset introduced using a delay line. The interferogram is of the form:

$$I(k) = \alpha(k)(1 - V \cos[kX - kx_e(k)]), \quad (\text{A1})$$

where $k = 2\pi/\lambda$ is the wavenumber; X is the displacement from zero optical path delay; $\alpha(k)$ is the source spectral envelope; V is the visibility; and $x_e(k)$ is the phase error that we want to measure. It is convenient to rewrite the above equation as

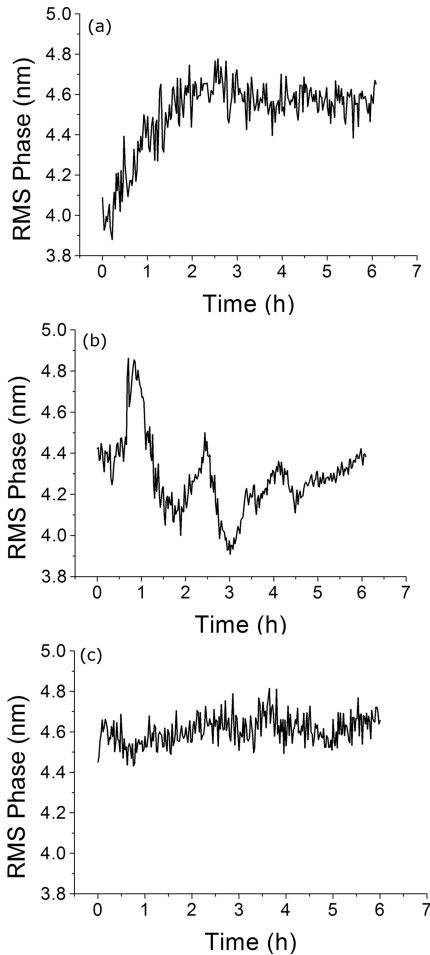


Fig. 10. RMS phase dispersion as a function of time for data sets (a) 1, (b) 2, and (c) 3.

$$I(k) = a(k) - \frac{1}{2} V a(k) e^{ikX - ikx_e(k)} - \frac{1}{2} V a(k) e^{-ikX + ikx_e(k)}. \quad (\text{A2})$$

We then perform a fast Fourier transform (FFT) on the interferogram to get

$$F\{I(k)\} = F\{a(k)\} - \frac{1}{2} V F\{a(k) e^{-ikx_e(k)}\} \times \delta(\lambda + X) - \frac{1}{2} V F\{a(k) e^{ikx_e(k)}\} \times \delta(\lambda - X), \quad (\text{A3})$$

where δ denotes the Kronecker delta function. If X is large then setting the negative frequency components and the near-DC components to zero eliminates the first two terms of the above equation. Performing an inverse FFT of the last term yields $(1/2) V a(k) e^{ikx_e(k)}$. The phase error term includes both the linear term caused by the OPD in the interferometer and the phase error of interest caused by the dis-

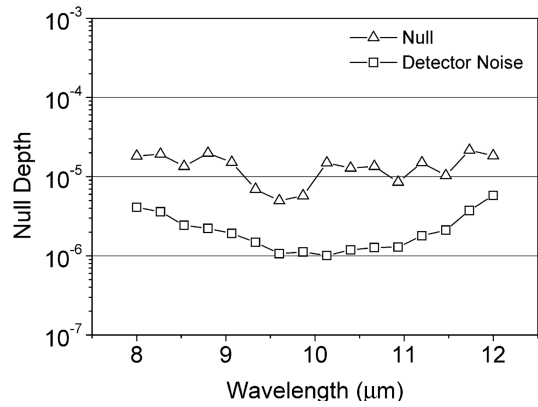


Fig. 11. Suppression of the signal after the correction to phase and intensity imbalance has been made.

persion in the optics. A polynomial fit to the phase obtained from the inverse FFT provides the phase error. The coefficient of the linear term gives an accurate measure of the OPD offset and is a confirmation of that set by the delay line.

The authors gratefully acknowledge the assistance Peter Lawson in the preparation of this paper. The work described in this paper was performed at the Jet Propulsion Laboratory, California Institute of Technology, under contract with the National Aeronautics and Space Administration.

References

1. E. Serabyn, "Nulling interferometry progress," *Proc. SPIE* **4838**, 594–608 (2003).
2. C. V. M. Fridlund and P. Gondoin, "The Darwin mission," *Proc. SPIE* **4852**, 394–404 (2003).
3. C. A. Beichman, N. J. Woolf, and C. A. Lindensmith, eds. *Terrestrial Planet Finder* (Jet Propulsion Laboratory, 1999).
4. P. R. Lawson, A. Ahmed, R. O. Gappinger, A. Ksendzov, O. P. Lay, S. R. Martin, R. D. Peters, D. P. Scharf, J. K. Wallace, and B. Ware, "Terrestrial planet finder technology status and plans," *Proc. SPIE* **6268**, 626828–626835 (2006).
5. J. K. Wallace, V. Babiwale, R. Bartos, K. Brown, R. Gappinger, F. Loya, D. MacDonald, S. Martin, J. Negron, T. Troung, and G. Vasisht, "Mid-IR interferometric nulling for TPF," *Proc. SPIE* **5491**, 862–873 (2004).
6. O. P. Lay, "Removing instability noise in nulling interferometers," *Proc. SPIE* **6268**, 62681A1–62681A3 (2006).
7. R. D. Peters, A. Hirai, M. Jeganathan, and O. P. Lay, "Adaptive nulling with a deformable mirror in the near-IR," *Proc. SPIE* **5905**, 590507-1–590507-8 (2005).
8. A. Ksendzov, O. Lay, S. Martin, J. S. Sanghera, L. E. Busse, W. H. Kim, P. C. Pureza, V. Q. Nguyen, and I. D. Aggarwal, "Characterization of mid-infrared single mode fibers as modal filters," *Appl. Opt.* **46**, 7957–7962 (2007).
9. R. N. Bracewell, *The Fourier Transform and Its Applications* (McGraw-Hill, 1986).